Vapor Deposited Photocatalytic Zeolitic Imidazolate Framework-8 Derived from Porous ZnO Thin Films

Marianne Kräuter[1], Katrin Unger[1,2], Roland Resel[1], Anna Maria Coclite[1,*]

[1] Institute of Solid State Physics, NAWI Graz, Graz University of Technology, Petersgasse 16, 8010 Graz, Austria
[1] Electronic Sensors, Silicon Austria Labs GmbH, Sandgasse 34, 8010 Graz, Austria
* e-mail: anna.coclite@tugraz.at

Table S1. Thickness of porous ZnO thin films with an open porosity of 14.5% - 24% and thickness of ZIF-8 synthesized from the ZnO, as measured via spectroscopic ellipsometry (SE) and profilometry.
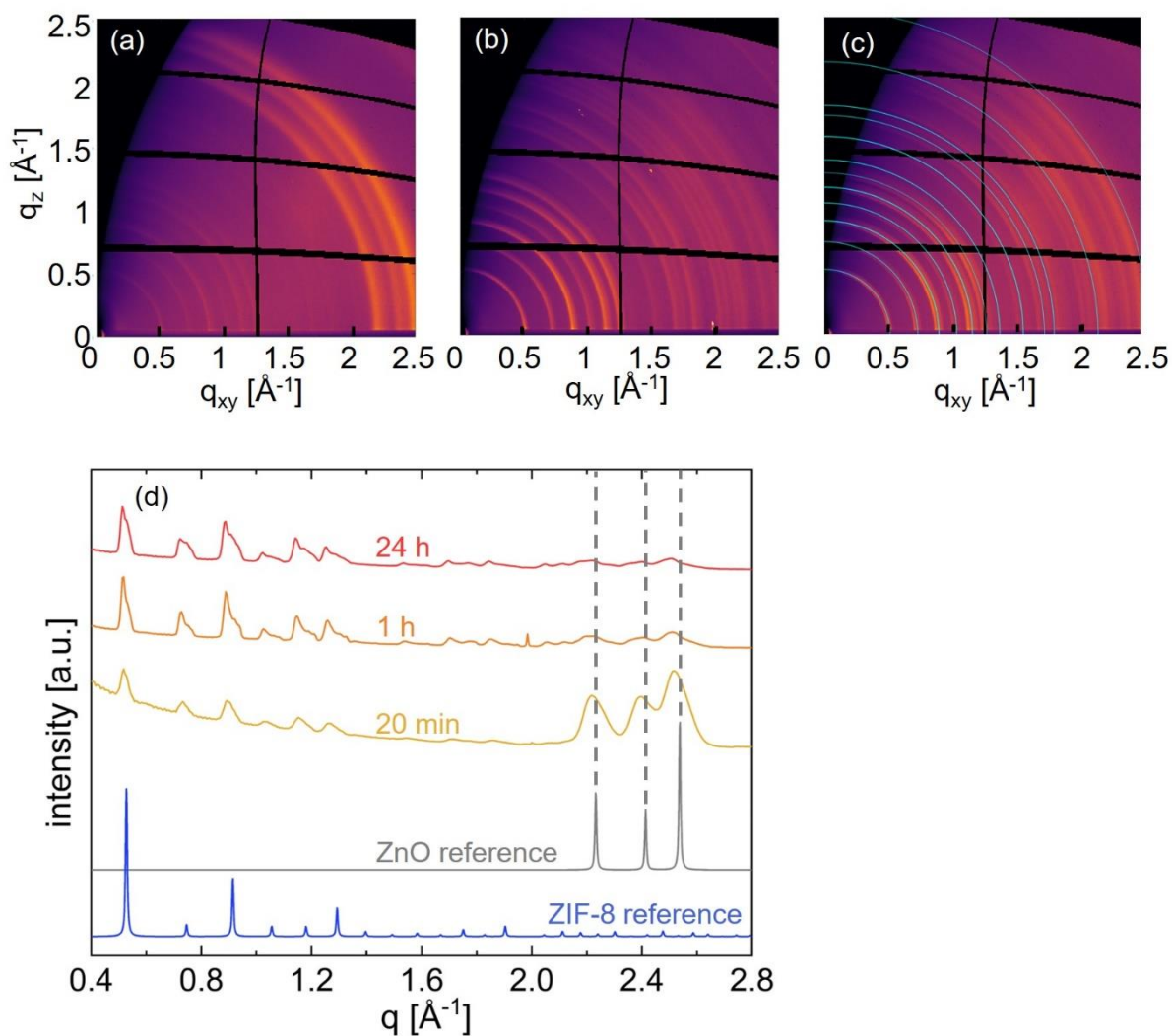*porosity. [%] … open porosity of the ZnO thin films in percent*
d_{ZnO} (SE) [nm]… thickness of porous ZnO in nanometer as measured via spectroscopic ellipsometry
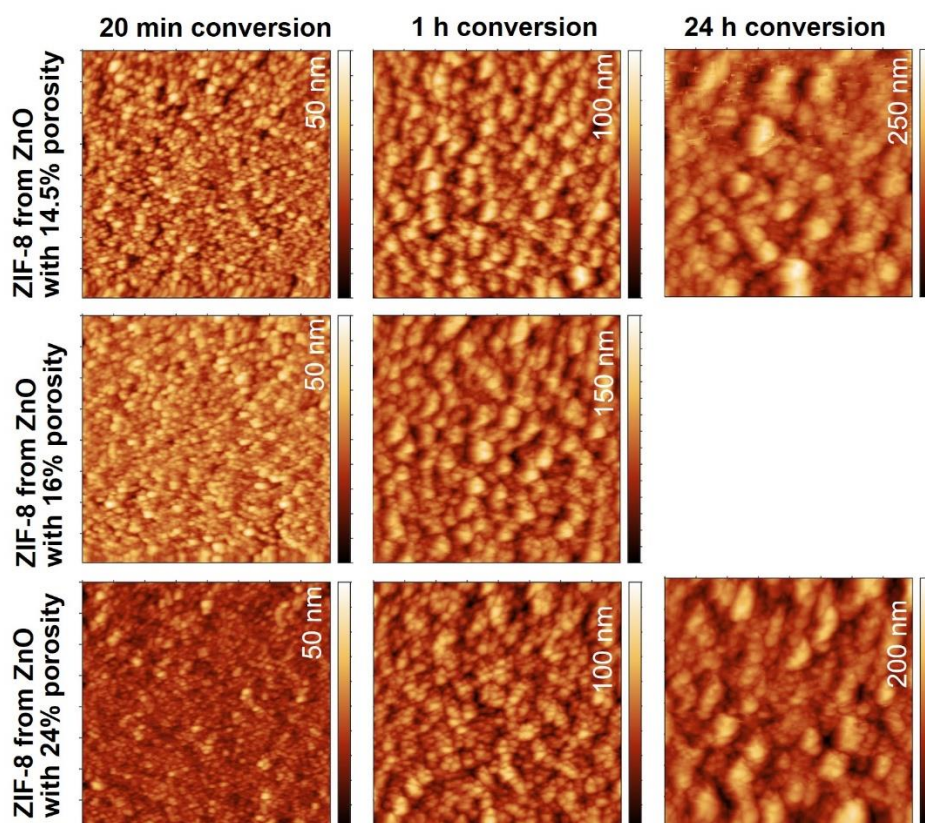*$t_{conv.}$ [min]… employed conversion time to obtain ZIF-8 from the ZnO thin films in minutes*
d_{ZIF-8} (SE / profilometry) [nm]… thickness of ZIF-8 obtained from porous ZnO in nanometer as measured via spectroscopic ellipsometry / profilometry

porosity [%]	d_{ZnO} (SE) [nm]	$t_{conv.}$ [min]	d_{ZIF-8} (SE) [nm]	d_{ZIF-8} (profilometry) [nm]
14.5	17 ± 2	20	22 ± 2	/
		60	135 ± 15	131 ± 16
		1440	172 ± 20	158 ± 2
16	16 ± 2	20	20 ± 2	/
		60	134 ± 15	130 ± 10
		1440	150 ± 20	/
24	15 ± 3	20	19 ± 2	/
		60	93 ± 15	/
		1440	132 ± 20	120 ± 12

Figure S1. Grazing X-Ray diffraction (GIXD) data of ZIF-8 converted from ZnO with (**a,b**) 16% open porosity for (**a**) 20 min and (**b**) 60 min. (**c**) GIXD image of ZIF-8 obtained from ZnO with 24% open porosity. indexed with a powder reference of ZIF-8 [43]. (**d**) shows line scans of grazing incidence X-ray diffraction (GIXD) measurements of ZIF-8 grown for 20 min to 24 h from ZnO with an open porosity of 24%. Powder reference patterns of ZnO and ZIF-8 are shown for comparison [43, 45].
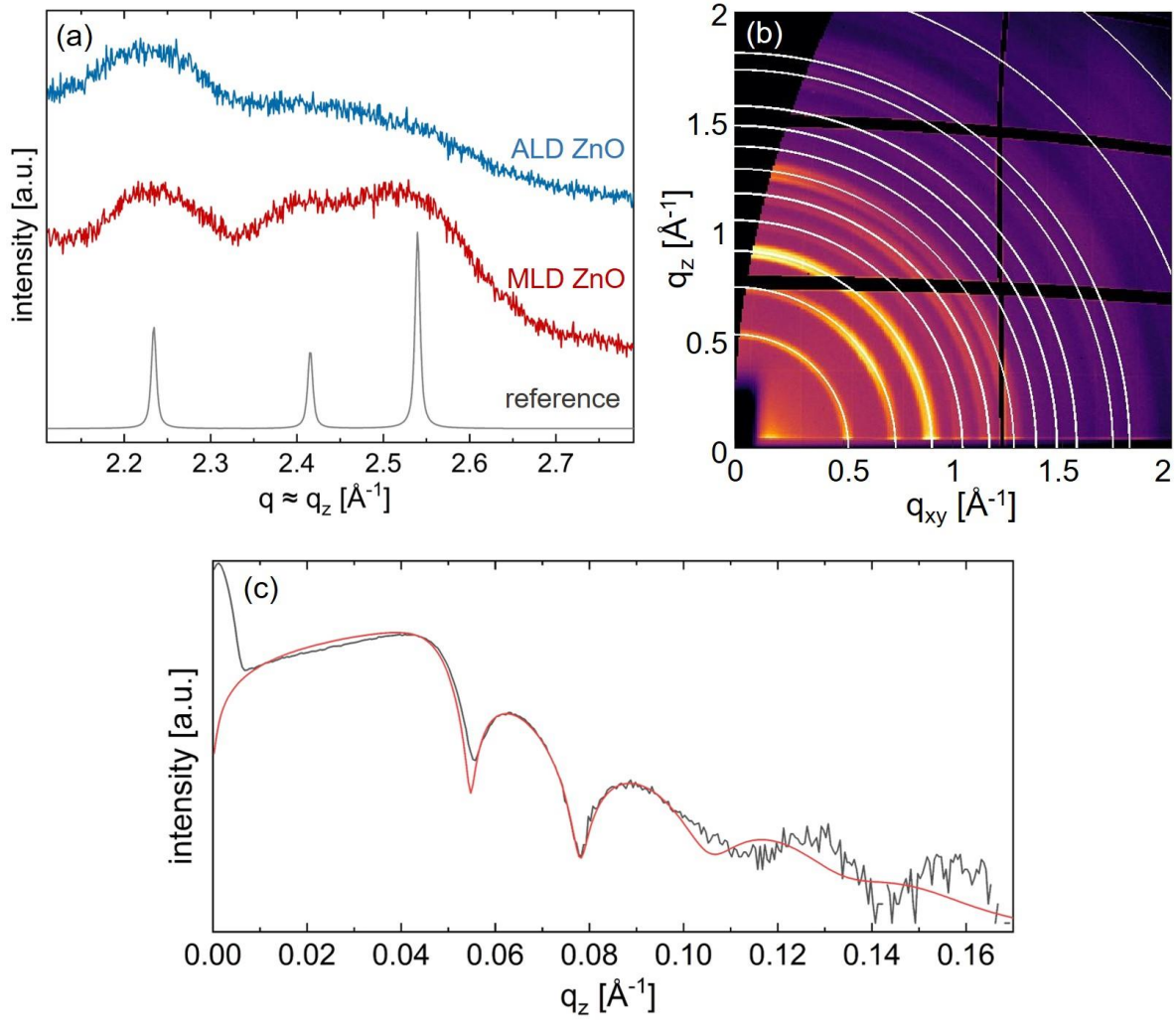
Figure S2. Atomic force microscopy images of ZIF-8 obtained after different conversion times from porous ZnO layers. All images are 8x8 μm in size; the color scale of each image has been individually adjusted for sake of visibility.

The samples employed for the photocatalytic tests were measured with SE to assess their thickness. The thicknesses resulted in (23 ± 3) nm for the ALD ZnO sample and to (17 ± 2) nm for the MLD ZnO sample. The thickness of the non-porous ZnO used for conversion of the ALD ZIF-8 sample was determined to (9.1 ± 0.5) nm and the thickness of the resulting ALD ZIF-8 sample to (150 ± 20) nm, resulting in a ~13-fold thickness increase. The SE values of the MLD ZIF-8 sample used for the photocatalytic tests are reported in the main file in Figure 4a,b.

Additionally, to prove the successful synthesis of the ZnO and ZIF-8 employed for the photocatalytic tests, XRD measurements were performed for the ALD ZnO (Figure S3a), the MLD ZnO sample (Figure S3a) and the MLD ZIF-8 sample (Figure 6b in the main file). The successful synthesis of the ALD ZIF-8 is shown via a GIXD image, that has been indexed with the polycrystalline structure of ZIF-8 (Figure S3b).

The density of the employed ALD ZnO sample was determined to (5.1 ± 0.3) g/cm^3 via XRR (Figure S3c). The fit yielded a roughness of (1.9 ± 0.5) nm and a thickness of (19 ± 2) nm, corroborating with the SE result. The density of MLD ZnO is reported in the main file (Figure 2b).
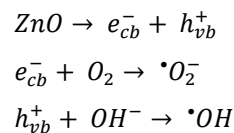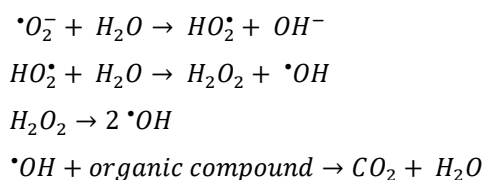
Figure S3. Investigation of the samples employed for photocatalytic tests with X-ray methods. (**a**) X-ray diffraction of non-porous ZnO obtained via plasma enhanced atomic layer deposition ("ALD ZnO") and of porous ZnO (16% open porosity) obtained via calcination of molecular layer deposited zincone ("MLD ZnO"). The "reference"-line on the bottom shows the peak positions of a ZnO powder reference [45]. (**b**) Grazing incidence X-ray diffraction of a ZIF-8 sample converted from ALD ZnO, indexed with a powder reference of ZIF-8 [43]. (**c**) X-ray reflectivity measurement of the non-porous ALD ZnO thin film. Red line corresponds to fit.

The photocatalytic degradation of methylene blue (MB) in presence of ZnO and ZIF-8 has been the subject of previous investigations and the corresponding reaction mechanisms have been proposed.
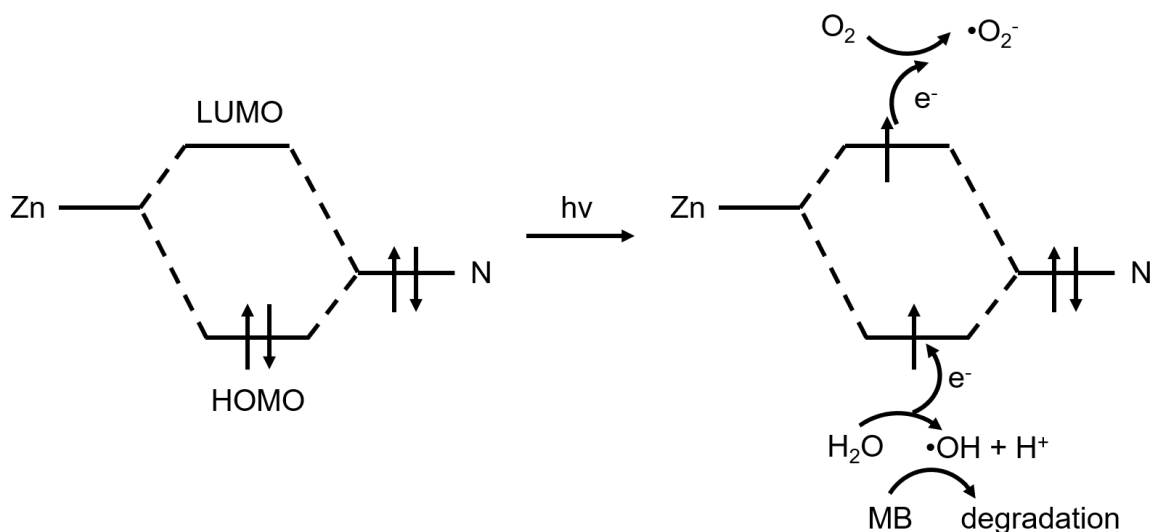
1) For ZnO [47]:

When the ZnO absorbs photons with an energy equal to or greater than its band gap, electrons (e-) of the valence band are promoted to the conduction band, which leaves a hole (h+) in the valence band. The photogenerated e- and h+ arrive at the surface of the ZnO and facilitate oxidation and reduction reactions, e.g. generating superoxide anions ($O_2^-\bullet$) and hydroxyl radicals. Subsequently, these highly reactive radical groups oxidize organic pollutant molecules in solutions. This process can be expressed also via chemical reactions, in which h^+_{vb} and e^-_{cb} represent the electron vacancies in the valence band and the electron in the conduction band, respectively:

$$ZnO \rightarrow e^-_{cb} + h^+_{vb}$$
$$e^-_{cb} + O_2 \rightarrow {}^\bullet O_2^-$$
$$h^+_{vb} + OH^- \rightarrow {}^\bullet OH$$

$$\cdot O_2^- + H_2O \rightarrow HO_2^{\bullet} + OH^-$$

$$HO_2^{\bullet} + H_2O \rightarrow H_2O_2 + \,^{\bullet}OH$$

$$H_2O_2 \rightarrow 2\,^{\bullet}OH$$

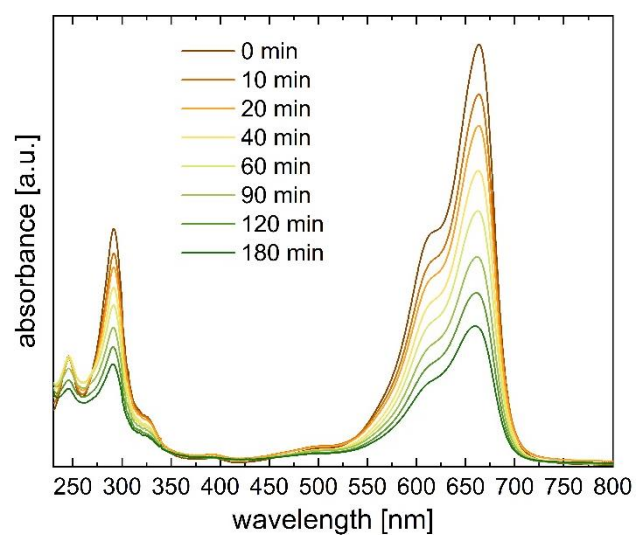$$^{\bullet}OH + organic\ compound \rightarrow CO_2 + H_2O$$

2) For ZIF-8 [29]:

Let us consider the highest occupied molecular orbital (HOMO) of ZIF-8, which is mainly formed by N 2p orbitals, and the lowest unoccupied molecular orbital (LUMO), formed by empty Zn orbitals. In the presence of UV light, an electron is transferred from the HOMO to the LUMO. The electrons of the excited state in the LUMO are easily lost to reactions in the aqueous solution, while the HOMO demands an electron to return to its stable state and captures this electron from the water in the solution. This results in oxygenation of the water molecule into the •OH active species, which can then decompose MB. Figure S4 shows a simplified model of the photocatalytic reaction mechanism of MB on ZIF-8.

Figure S4. A simplified model of the photocatalytic reaction mechanism of methylene blue on ZIF-8. The depiction has been adapted from literature [29].

Figure S5. UV-vis absorption spectra of a 10^{-5} mol/l methylene blue solution in the presence of ZIF-8 under UV irradiation. The same data is displayed in Figure 5a; however, here the x-axis has been extended down to 230 nm to demonstrate the behavior of absorption peaks at lower wavelengths.